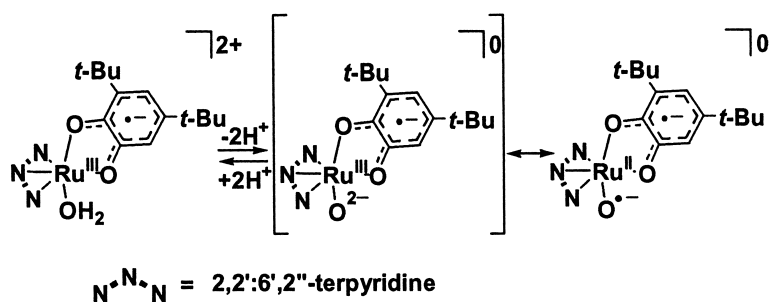Article

Characterization of a Stable Ruthenium Complex with an Oxyl Radical

Katsuaki Kobayashi, Hideki Ohtsu, Tohru Wada, Tatsuhisa Kato, and Koji Tanaka

More About This Article

Additional resources and features associated with this article are available within the HTML version:

- Supporting Information
- Links to the 7 articles that cite this article, as of the time of this article download
- Access to high resolution figures
- Links to articles and content related to this article
- Copyright permission to reproduce figures and/or text from this article

View the Full Text HTML

Characterization of a Stable Ruthenium Complex with an Oxyl Radical

Katsuaki Kobayashi, Hideki Ohtsu, Tohru Wada, Tatsuhisa Kato, and Koji Tanaka*
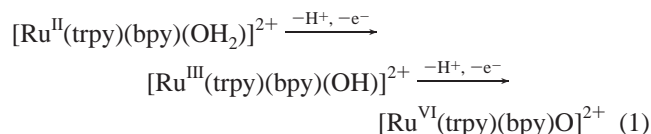
Contribution from the Institute for Molecular Science, CREST, Japan Science and Technology Corporation, Department of Structural Molecular Science, The Graduate University for Advanced Studies, 38 Nishigonaka, Myodaiji, Okazaki, Aichi 444-8585, Japan

Received September 5, 2002; E-mail: ktanaka@ims.ac.jp

Abstract: The ruthenium oxyl radical complex, [Ru^{II}(trpy)(Bu$_2$SQ)O$^{•-}$] (trpy = 2,2':6',2''-terpyridine, Bu$_2$-SQ = 3,5-di-*tert*-butyl-1,2-benzosemiquinone) was prepared for the first time by the double deprotonation of the aqua ligand of [Ru^{III}(trpy)(Bu$_2$SQ)(OH$_2$)](ClO$_4$)$_2$. [Ru^{III}(trpy)(Bu$_2$SQ)(OH$_2$)](ClO$_4$)$_2$ is reversibly converted to [Ru^{III}(trpy)(Bu$_2$SQ)(OH$^-$)]$^+$ upon dissociation of the aqua proton (pK_a 5.5). Deprotonation of the hydroxo proton gave rise to intramolecular electron transfer from the resultant O^{2-} to Ru−dioxolene. The resultant [Ru^{II}(trpy)(Bu$_2$SQ)O$^{•-}$] showed antiferromagnetic behavior with a Ru^{II}−semiquinone moiety and oxyl radical, the latter of which was characterized by a spin trapping technique. The most characteristic structural feature of [Ru^{II}(trpy)(Bu$_2$SQ)O$^{•-}$] is a long Ru−O bond length (2.042(6) Å) as the first terminal metal−O bond with a single bond length. To elucidate the substituent effect of a quinone ligand, [Ru^{III}(trpy)(4ClSQ)(OH$_2$)]-(ClO$_4$)$_2$ (4ClSQ = 4-chloro-1,2-benzosemiquinone) was prepared and we compared the deprotonation behavior of the aqua ligand with that of [Ru^{III}(trpy)(Bu$_2$SQ)(OH$_2$)](ClO$_4$)$_2$. Deprotonation of the aqua ligand of [Ru^{III}(trpy)(4ClSQ)(OH$_2$)](ClO$_4$)$_2$ induced intramolecular electron transfer from OH$^-$ to the [Ru^{III}-(4ClSQ)] moiety affording [Ru^{II}(trpy)(4ClSQ)(OH$^•$)]$^+$, which then probably changed to [Ru^{II}(trpy)(4ClSQ)O$^{•-}$]. The antiferromagnetic interactions (*J* values) between Ru^{II}-semiquinone and the oxyl radical for [Ru^{II}(trpy)(Bu$_2$SQ)O$^{•-}$] and for [Ru^{II}(trpy)(4ClSQ)O$^{•-}$] were 2J = −0.67 cm^{-1} and −1.97 cm^{-1}, respectively.

Introduction

The reactivity of high-valent metal-oxo complexes is of current interest from the viewpoint of enzymatic activation of dioxygen on metals via O$_2$ binding, O$_2$ reduction, and oxidation or oxygenation of organics by such as P-450 enzymes.[1] Mechanistic understandings of the reactivity of O$_2$ on metals have, however, been limited because of the difficulty of selective cleavage of the O−O bond of O$_2$ on metals in artificial systems. Instead, high-valent Ru=O complexes have been extensively studied, since oxidation of Ru−OH$_2$ complexes affords higher oxidation states of Ru−OH and Ru=O complexes by sequential electron and proton loss (eq 1).[2]

$$[Ru^{II}(trpy)(bpy)(OH_2)]^{2+} \xrightarrow{-H^+, -e^-}$$
$$[Ru^{III}(trpy)(bpy)(OH)]^{2+} \xrightarrow{-H^+, -e^-}$$
$$[Ru^{VI}(trpy)(bpy)O]^{2+} \quad (1)$$

Indeed, a variety of high-valent Ru=O complexes have been prepared by treatment of Ru−OH$_2$ complexes with Ce(IV),[3] and some of them have proven to work as oxidants.[4] The accessibility to the higher oxidation states of Ru complexes are attributed to electron donation from bound oxo ligands. Dioxolene is an electrochemically noninnocent ligand and takes three different electronic states classified as quinone (Q), semiquinone (SQ), and catecholate (Cat). The noticeable feature of metal−dioxolene complexes, therefore, is the charge distribution between the central metal ions and the ligands on account of accessible reduction states of dioxolene.[5−11] As for total six

(1) (a) Watanabe, Y. *J. Biol. Inorg. Chem.* **2001**, *6*, 846. (b) Sano, M.; Roach, M. P.; Coulter, E. D.; Dawson, J. H. *Chem. Rev.* **1996**, *96*, 2841.

(2) (a) Moyer, B. A.; Meyer, T. J. *Inorg. Chem.* **1981**, *20*, 436. (b) Takeuchi, K. J.; Thompson, M. S.; Pipes, D. W.; Meyer, T. J. *Inorg. Chem.* **1984**, *23*, 1845.

(3) (a) Szczepura, L. F.; Maricich, S. M.; See, R. F.; Churchill, M. R.; Takeuchi, K. J. *Inorg. Chem.* **1995**, *34*, 4198. (b) Che, C.-M.; Tang, W.-T.; Wong, W.-T.; Lai, T.-F. *J. Am. Chem. Soc.* **1989**, *111*, 9048. (c) Geselowiz, D.; Meyer, T. J. *Inorg. Chem.* **1990**, *29*, 3894.

(4) (a) Acquaye, J. H.; Muller, J. G.; Takeuchi, K. J. *Inorg. Chem.* **1993**, *32*, 160. (b) Lebeau, E. L.; Meyer, T. J. *Inorg. Chem.* **1999**, *38*, 2174. (c) Che, C.-M.; Tang, W.-T.; Lee, W.-O.; Wong, K.-Y.; Lau, T.-C. *J. Chem. Soc., Dalton Trans.* **1992**, 1551. (d) Seok, W. K.; Dobson, J. C.; Meyer, T. J. *Inorg. Chem.* **1988**, *27*, 3. (e) Che, C.-M.; Ho, C.; Lau, T.-C. *J. Chem. Soc., Dalton Trans.* **1991**, 1259. (f) Fung, W.-H.; Yu, W.-Y.; Che, C.-M. *J. Org. Chem.* **1998**, *63*, 7715. (g) Labeau, E. L.; Adeyemi, S. A.; Meyer, T. J. *Inorg. Chem.* **1998**, *37*, 6476. (h) Moyer, B. A.; Sipe, B. K.; Meyer, T. J. *Inorg. Chem.* **1981**, *20*, 1475. (i) Stultz, L. K.; Binstead R. A.; Reynolds, M. S.; Meyer, T. J. *J. Am. Chem. Soc.* **1995**, *117*, 2520. (j) Roecker, L.; Meyer, T. J. *J. Am. Chem. Soc.* **1987**, *109*, 746. (k) Dovletoglou, A.; Meyer, T. J. *J. Am. Chem. Soc.* **1994**, *116*, 215.

(5) (a) Pierpont, C. G.; Buchanan, R. M. *Coord. Chem. Rev.* **1981**, *38*, 45. (b) Pierpont, C. G.; Lange, C. W. *Prog. Inorg. Chem.* **1994**, *41*, 331.

(6) (a) Haga, M.; Dodsworth, E. S.; Lever, A. P. B.; Boone, S. R.; Pierpont, C. G. *J. Am. Chem. Soc.* **1986**, *108*, 7413. (b) Boone, S. R.; Pierpont, C. G. *Inorg. Chem.* **1987**, *26*, 1769. (c) Bhattacharya, S.; Pierpont, C. G. *Inorg. Chem.* **1991**, *30*, 1511. (d) Bhattacharya, S.; Pierpont, C. G. *Inorg. Chem.* **1992**, *31*, 35. (e) Bhattacharya, S.; Pierpont, C. G. *Inorg. Chem.* **1994**, *33*, 6038. (f) Sugimoto, H.; Tanaka, K. *J. Organomet. Chem.* **2001**, *622*, 280.

(7) (a) Haga, M.; Dodsworth, E. S.; Lever, A. P. B. *Inorg. Chem.* **1986**, *25*, 447. (b) Ebadi, M.; Lever, A. P. B. *Inorg. Chem.* **1999**, *38*, 467.

(8) (a) Lever, A. P. B.; Auburn, P. R.; Dodsworth, E. S.; Haga, M.; Liu, W.; Melnik, M.; Nevin, W. A. *J. Am. Chem. Soc.* **1988**, *110*, 8076. (b) Auburn, P. R.; Dodsworth, E. S.; Haga, M.; Liu, W.; Nevin, W. A.; Lever, A. P. B. *Inorg. Chem.* **1991**, *30*, 3502.

oxidation states of Ru^{II}− and Ru^{III}−dioxolene complexes, the actual structures of [Ru^{II}(Q)] and [Ru^{III}(SQ)] complexes and those of [Ru^{II}(SQ)] and [Ru^{III}(Cat)] ones are expressed as resonance hybrids between two complexes (eqs 2 and 3).

$$[Ru^{II}(Q)] \leftrightarrow [Ru^{III}(SQ)] \qquad (2)$$
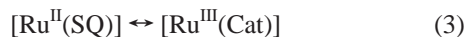
$$[Ru^{II}(SQ)] \leftrightarrow [Ru^{III}(Cat)] \qquad (3)$$

The C−O bond lengths of dioxolene ligands and XPS of Ru atoms have been used as criteria for determining whether the resonances of eqs 2 and 3 lie to the two extremes. As for the resonance of eq 3, a number of [Ru^{II}(SQ)] and [Ru^{III}(Cat)] complexes have been documented so far. On the other hand, there has been reported only one example of a [Ru^{III}(SQ)] complex with regard to the resonance of eq 2.[12]

Taking into account that higher oxidation states of Ru=O complexes have been obtained by the oxidation of central metals coupled with deprotonation of Ru−OH$_2$ ones, we believe the introduction of dioxolene ligands as an electron acceptor into the Ru−OH$_2$ framework would induce deprotonation of the aqua ligand without using oxidants to oxidize the central Ru ion. Such redox reactions of dioxolene driven by deprotonation of aqua-Ru−dioxolene complexes would serve not only a smooth conversion from aqua- to oxo-group on Ru but also the development of a new type of electrocatalysis.[13] Recently, we briefly reported deprotonation behavior of Ru aqua complexes with a quinone ligand[13] and participation of an oxyl radical intermediate in the four-electron oxidation of water[15] and dehydrogenation of cyclic dienes[15] catalyzed by mono- and dinuclear aqua-Ru−dioxolene complexes.

In this work, we prepared the Ru−dioxolene complexes, [Ru^{II}(trpy)(Bu$_2$SQ)(OAc)] (**1**) (trpy = 2,2′:6′,2″-terpyridine, Bu$_2$SQ = 3,5-di-*tert*-1,2-benzosemiquinone), [Ru^{II}(trpy)(4ClSQ)-(OAc)] (**2**) (4ClSQ = 4-chloro-1,2-benzosemiquinone), [Ru^{III}-(trpy)(Bu$_2$SQ)(OH$_2$)](ClO$_4$)$_2$ (**3**), [Ru^{III}(trpy)(4ClSQ)(OH$_2$)]-(ClO$_4$)$_2$ (**4**), and [Ru^{II}(trpy)(Bu$_2$SQ)O$^{\bullet-}$] (**5**). The crystal structures of **1**, **3**, and the biradical complex **5** as the doubly deprotonated form of complex **3** are reported. In addition, deprotonation behavior of the aqua ligand of **3** is compared with that of **4**. Electronic states of biradical complexes [Ru^{II}(trpy)(Bu$_2$SQ)O$^{\bullet-}$] and [Ru^{II}(trpy)(4ClSQ)O$^{\bullet-}$] are also discussed.

Experimental Section

Materials. 2-Methoxyethanol solutions of *t*-BuOK and HClO$_4$ (0.1 M) were used as a base and an acid. Dichloromethane solutions of DMPO (5,5-dimethyl-1-pyrroline *N*-oxide) (0.1 M) were used as stock solutions of spin trapping reagents.

(Caution: All the perchlorate salts are explosive and should be handled with care!)

Preparations. Preparation of [Ru^{II}(trpy)(Bu$_2$SQ)(OAc)] has been reported elsewhere,[16] but a little modification was carried out to improve the yields and purity of the complex, because the reaction of catechol with [Ru^{III}(trpy)Cl$_3$] in methanol gave a mixture of [Ru^{II}(trpy)(R$_n$SQ)-Cl] and [Ru^{II}(trpy)(R$_n$SQ)(OAc)].

[Ru^{II}(trpy)(Bu$_2$SQ)(OAc)] (1). A mixture of [Ru^{III}(trpy)Cl$_3$] (500 mg, 1.14 mmol) and AgBF$_4$ (662 mg, 3.40 mmol) in acetone (50 mL) was refluxed for 2 h.[17] After removal of AgCl by filtration, the filtrate was evaporated under reduced pressure. The residue and 3,5-di-*tert*-butylcatechol (252 mg, 1.14 mmol) were dissolved in deaerated methanol (30 mL), and then potassium acetate (1.11 g, 11.4 mmol) in methanol (20 mL) was added to the solution under N$_2$. The mixture was stirred for 24 h at room temperature. The resulting purple solution was evaporated under reduced pressure, and the residue was extracted with acetone to remove excess potassium acetate. The acetone solution was loaded on a silica gel column. After [Ru^{III}(Bu$_2$SQ)$_3$] was eluted with acetone, [Ru^{II}(trpy)(Bu$_2$SQ)(OAc)] (**1**) adsorbed on the top of the column was eluted with methanol. Violet plates of **1** crystallized out of the solution and were separated by filtration. Yield 304 mg (43.7%). Anal. Calcd for C$_{31}$H$_{38}$N$_3$O$_6$Ru: C, 57.31; H, 5.91; N, 6.47. Found: C, 57.20; H, 6.53; N, 6.26.

[Ru^{II}(trpy)(4ClSQ)(OAc)] (2).[18] This complex was prepared in a procedure analogous to that described previously for **1**. Yield 314 mg (51.6%). Anal. Calcd for C$_{23}$H$_{19}$N$_3$O$_5$ClRu: C, 49.87; H, 3.45; N, 7.58. Found: C, 50.16; H, 3.32; N, 7.67.

[Ru^{III}(trpy)(Bu$_2$SQ)(OH$_2$)](ClO$_4$)$_2$ (3).[19] Aqueous HClO$_4$ (70%, 0.25 mL) was added to a methanolic solution (10 mL) of **1** (50 mg, 0.081 mmol). The resultant deep blue solution was stirred overnight at room temperature. After 100 mg of sodium perchlorate and 10 mL of water were added to the solution, the mixture was allowed to stand at room temperature for a week. Deep blue needles of **3** crystallized out of the solution and were separated by filtration. Yield 38.8 mg (61.7%). Anal. Calcd for C$_{29}$H$_{35}$N$_3$O$_{12}$Cl$_2$Ru: C, 44.11; H, 4.47; N, 5.32. Found: C, 44.37; H, 4.39; N, 5.31.

[Ru^{III}(trpy)(4ClSQ)(OH$_2$)](ClO$_4$)$_2$ (4). Aqueous HClO$_4$ (70%, 0.25 mL) was added to a water/ethylene glycol dimethyl ether solution (1:1 v/v, 6 mL) of **2** (53 mg, 0.080 mmol). The resultant blue purple solution was stirred overnight at room temperature. The volume of the solvent was reduced to about one-forth under N$_2$ gas flow. Dark purple **4** precipitated out of the solution and was separated by filtration. Yield 32.0 mg (48.9%). Anal. Calcd for C$_{21}$H$_{20}$N$_3$O$_{13}$Cl$_3$Ru: C, 34.56; H, 2.76; N, 5.76. Found: C, 34.65; H, 2.39; N, 5.79.

[Ru^{II}(trpy)(Bu$_2$SQ)O$^{\bullet-}$] (5). A water/methanol solution (1:1 v/v, 40 mL) of **3** (50 mg 0.065 mmol) was dropped to an aqueous NaOH solution (4 M, 20 mL), and the solution was stirred overnight. Then, the solution was allowed to stand under N$_2$ flow. Reddish purple needles of **5** crystallized out of the solution, were separated by filtration, and washed with cold water. Yield 16.8 mg (45.6%). Anal. Calcd for C$_{29}$H$_{33}$N$_3$O$_4$Ru: C, 59.17; H, 5.65; N, 7.14. Found: C, 59.02; H, 5.81; N, 7.07.

Instruments. Electronic absorption spectra were recorded on a Shimadzu UV-3100PC spectrometer at 298 K. pH value of aqueous solutions were measured with a pH meter (Scientific Instruments IQ240). Cyclic voltammograms of the complexes were obtained in CH$_2$-Cl$_2$ containing 0.1 M of tetra-*n*-butylammonium perchlorate (TBAP) as a supporting electrolyte at 298 K by using three electrodes under N$_2$ and an ALS/chi Electrochemical Analyzer model 660. A glassy-carbon plate and platinum wire were used as a working electrode and a counter electrode, respectively. All potentials were recorded against an SCE reference electrode.

Resonance Raman spectra were obtained using an excitation at 632.8 nm with an He−Ne laser or at 704.3 nm with a DCM dye laser and detected with a JASCO NR-1800 triple polychromator equipped with

(9) Bag, N.; Pramanik, A.; Lahiri, G. K.; Chakravorty, A. *Inorg. Chem.* **1992**, *31*, 40.

(10) Masui, H.; Lever, A. B. P.; Auburn, P. R. *Inorg. Chem.* **1991**, *30*, 2402.

(11) Buttacharyya, I.; Shivakumar, M.; Chakravorty, A. *Polyhedron* **2002**, *21*, 2761.

(12) Boone, S. R.; Pierpont, C. G. *Polyhedron* **1990**, *9*, 2267.

(13) Kobayashi, K.; Ohtsu, H.; Wada, T.; Tanaka, K. *Chem. Lett.* **2002**, 868.

(14) Wada, T.; Tsuge, K.; Tanaka, K. *Chem. Lett.* **2000**, 910.

(15) (a) Wada, T.; Tsuge, K.; Tanaka, K. *Angew. Chem., Int. Ed.* **2000**, *39*, 1479. (b) Wada, T.; Tsuge, K.; Tanaka, K. *Inorg. Chem.* **2001**, *40*, 329.

(16) Kurihara, M.; Daniele, S.; Tsuge, K.; Sugimoto, H.; Tanaka, K. *Bull. Chem. Soc. Jpn.* **1998**, *71*, 867.

(17) Gourdon, A.; Launay, J.-P. *Inorg. Chem.* **1998**, *37*, 5336.

(18) The Ru 3d$_{5/2}$ binding energy of **2** was 280.4 eV due to the Ru^{II} core (Table 3).

(19) (a) Tsuge, K.; Tanaka, K. *Chem. Lett.* **1998**, 1069. (b) Tsuge, K.; Kurihara, M.; Tanaka, K. *Bull. Chem. Soc. Jpn.* **2000**, *73*, 607.

Table 1. Crystallographic Data for Complexes **1**, **3**, and **5**

	1	3	5
formula	$C_{32}H_{37}N_3O_5Ru$	$C_{29}H_{31}N_3O_{12}RuCl_2$	$C_{29}H_{31}N_3O_7Ru$
formula weight	644.73	785.55	634.65
color	violet	blue	reddish purple
crystal size/mm^3	$0.50 \times 0.30 \times 0.20$	$0.20 \times 0.06 \times 0.06$	$0.20 \times 0.10 \times 0.10$
crystal system	triclinic	triclinic	tetragonal
space group	$P\text{-}1$	$P\text{-}1$	$I\text{-}4$
a/Å	8.391(5)	10.989(2)	24.688(2)
b/Å	9.318(6)	11.062(2)	24.688(2)
c/Å	21.46(2)	15.058(2)	10.0934(9)
α/deg	86.59(2)	91.681(4)	90
β/deg	81.85(2)	103.517(5)	90
γ/deg	65.66(1)	109.252(6)	90
V/Å^3	1513(1)	1668.9(5)	6152.0(8)
Z	2	2	8
T/K	173	173	173
D_{calc}/g cm^{-3}	1.415	1.563	1.370
radiation	Mo Kα ($\lambda = 0.710\,70$ Å)	Mo Kα ($\lambda = 0.710\,70$ Å)	Mo Kα ($\lambda = 0.710\,70$ Å)
μ/cm^{-1}	5.62	6.95	5.57
$F(000)$/e	668.00	800.00	2608.00
$2\theta_{max}$/deg	55.0	55.0	55.0
no. of reflections measured	6556	7302	3722
reflections used	6545	7214	3707
no. of variables	370	424	352
reflection/parameter ratio	17.69	17.01	10.53
GOF	1.890	1.605	0.855
R^a ($I > 2\sigma(I)$)	0.050	0.064	0.048
$R_w{}^a$ ($I > 2\sigma(I)$)	0.073	0.074	0.057

^{a} $R = \sum[|F_o| - |F_c|]/\sum|F_o|$; $R_w = [(\sum w(|F_o| - |F_c|))^2/\sum w(|F_o|^2)]^{1/2}$; $w = 1/\sigma^2(F_o)$.

a liquid nitrogen cooled Princeton Instruments CCD detector. Raman measurements were carried out with a spinning cell, and the laser power was adjusted to 7 mW (632.8 nm excitation) and 30 mW (704.3 nm excitation) at the sample point. Raman shifts were calibrated using dichloromethane with the accuracy of the peak positions of the Raman bands being ±1 cm^{-1}.

The EPR spectra at 193 K were measured with a JEOL X-band spectrometer (JES-RE1XE) using an attached VT (Variable Temperature) apparatus. The g values were calibrated precisely with an Mn^{2+} marker which was used as a reference. Frozen state EPR spectra at low temperatures were measured with a Brüker X-band spectrometer (Brüker ESP300E) attached to a cryostat (Oxford ESR900) and a temperature controller (Oxford Model ITC4). The g values were calculated from the magnetic field and the microwave frequency, measured by an NMR tesla meter (Brüker ER035M) and a microwave frequency counter (Hewlett Packard 5352B), respectively. Both of the measurements were demonstrated under nonsaturating microwave power conditions. The signal intensities around $g = 4$ were obtained by double integration of signals with computer calculation.

Electron spray mass spectra were obtained with a JEOL JMS-T100L attached to a syringe pump apparatus (Harvard Apparatus model 22). The ion spray interface was adjusted to 2.0 kV, and then sample solutions were loaded to the sprayer through a glass capillary ($\phi = 100\ \mu$m) at 10 μL/s. Nebulization of solutions were performed by compressed N$_2$. A TOF detector was employed to the ion detection in positive detection mode, whose detection range is 250–1000 (m/z). Orifice potential was maintained at 25 V.

X-ray photoelectron spectra (XPS) were recorded on a VG Scientific Ltd. ESCA LAB MK II. Mg Kα radiation (1253.6 eV) operated at 14.5 kV and 20 mA was used as an X-ray excitation source. All samples were deposit on gold foil from CH$_2$Cl$_2$ solutions. The C 1s peak was assigned as the value of 284.6 eV and used as the internal reference.

X-ray Crystallography. Data of **1**, **3**, and **5** were collected on a Rigaku/MSC Mercury CCD diffractometer using graphite monochromated Mo Kα radiation ($\lambda = 0.710\,70$ Å). To determine the cell constants and the orientation matrix, we generated four oscillation photographs with an oscillation angle of 0.5°. The images for intensity data were collected at a temperature of -100 ± 1 °C to a maximum

2θ value of 55.0°. Each image was taken twice and averaged. Finally, a total of 720 oscillation images were collected. The first sweep of data was done using ω scans from -70.0° to 110.0° in 0.5° steps, at $\chi = 45.0$° and $\phi = 0.0$°. The second sweep of data was done using ω scans from -70.0° to 110.0° in 0.5° steps, at $\chi = 45.0$° and $\phi = 90.0$°. The detector swing angle was 20.0°. The crystal-to-detector distance was 45.0 mm.

The structures were solved by heavy-atom Patterson methods[20] for **1** and direct method SIR92[21] for **3** and **5** and expanded using Fourier techniques.[22] The non-hydrogen atoms were refined anisotropically. Hydrogen atoms were included at geometrically determined positions (C–H 0.95 Å) but not refined. All calculations were performed using the teXsan[23] crystallographic software package of Molecular Structure Corporation. Crystallographic data are summarized in Table 1.
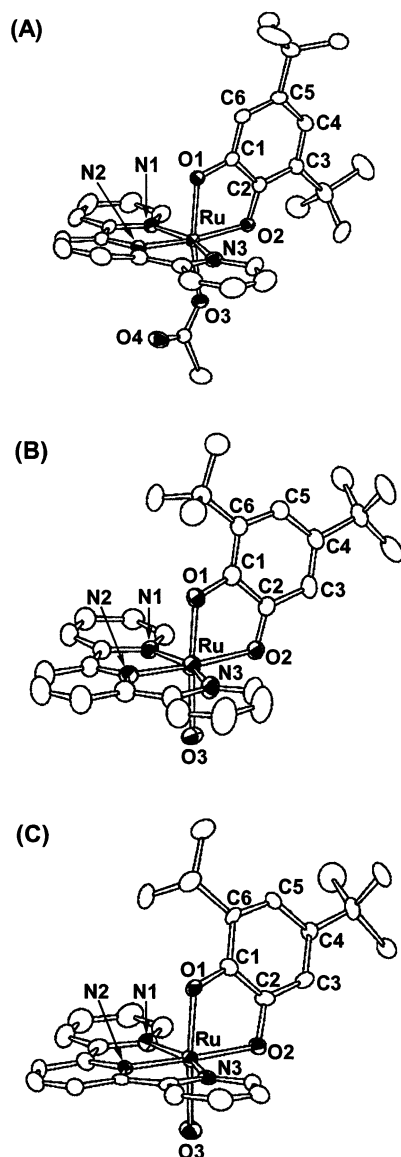
Results and Discussion

Preparation and Crystal Structures of [Ru^{II}(trpy)-(Bu$_2$SQ)(OAc)] (1), [Ru^{III}(trpy)(Bu$_2$Q)(OH$_2$)](ClO$_4$)$_2$ (3), and [Ru^{II}(trpy)(Bu$_2$SQ)O$^{\bullet-}$] (5). Hydrolysis of [Ru^{II}(trpy)-(Bu$_2$SQ)(OAc)] (**1**) under strong acidic conditions produced [Ru^{III}(trpy)(Bu$_2$SQ)(OH$_2$)]$^{2+}$ (**3**) (see the following), which was isolated as the blue violet single crystals of a perchlorate salt. The aqua complex **3** is soluble in H$_2$O, and the pK_a value of the aqua ligand was determined as 5.5 by means of pH titration and changes of the electronic absorption spectra in H$_2$O at 25 °C. We observed the occurrence of the second deprotonation of **3** at a pH higher than 10, but reddish purple solids precipitated out of the aqueous solution in that pH region. The doubly

(20) Beurskens, P. T.; Admiraal, G.; Beurskens, G.; Bosman, W. P.; de Gelder, R.; Israel, R.; Smits, J. M. M. PATTY; 1994.
(21) For SIR92, see: Altomare, A.; Burla, M. C.; Camalli, M.; Cascarano, M.; Giacovazzo, C.; Guagliardi, A.; Polidori, G. *J. Appl. Crystallogr.* **1994**, *27*, 435.
(22) Beurskens, P. T.; Admiraal, G.; Beurskens, G.; Bosman, W. P.; de Gelder, R.; Israel, R.; Smits, J. M. M. DIRDIF94; 1994. The DIRDIF-94 program system, Technical Report of the Crystallography Laboratory, University of Nijmegen, The Netherlands.
(23) teXsan: Crystal Structure Analysis Package, Molecular Structure Corporation (1985 and 1992).

(A)

(B)

(C)

Figure 1. Crystal structures of **1** (A), **3** (B), and **5** (C) with labeling for selected atoms. All hydrogen atoms are omitted for clarity.

Table 2. Selected Bond Lengths (Å) for Complexes **1**, **3**, and **5**

	1	3	5
Ru−O1	2.030(3)	1.968(3)	1.985(6)
Ru−O2	2.019(3)	2.028(3)	2.058(6)
Ru−O3	2.062(3)	2.099(3)	2.043(7)
Ru−N1	2.050(3)	2.063(4)	2.071(8)
Ru−N2	1.952(3)	1.959(4)	1.945(8)
Ru−N3	2.056(3)	2.059(4)	2.050(8)
C1−O1	1.328(4)	1.293(5)	1.35(1)
C2−O2	1.324(4)	1.280(5)	1.34(1)
C1−C2	1.430(5)	1.466(6)	1.43(1)
C2−C3	1.421(5)	1.420(6)	1.39(1)
C3−C4	1.392(5)	1.357(7)	1.38(1)
C4−C5	1.430(5)	1.454(6)	1.39(1)
C5−C6	1.383(5)	1.365(6)	1.39(1)
C6−C1	1.396(5)	1.423(6)	1.44(1)

Carbon−oxygen bond lengths of dioxolene ligands reflect the charge distribution of metal−dioxolene complexes.[5,6] The two C−O bond distances, C1−O1 and C2−O2, of the dioxolene ligands of **1**, **3**, and **5** are 1.328(4) and 1.324(4) Å, 1.293(5) Å and 1.280(5) Å, and 1.35(1) and 1.34(1) Å, respectively. Thus, the C−O bond distances of **1** and **5** are apparently longer than those of **3**. The latter is associated with coordinated semiquinone of $[Ru^{III}(3ClPy)_2(Bu_2SQ)_2]^+$ (3Clpy = 3-chloropyridine, 1.29 Å).[12] On the other hand, C−O bond lengths of $[Ru^{II}(Bu_2SQ)]$ complexes vary in wide ranges; for example, $[Ru^{II}(Bu_2SQ)$-$(Cl)(CO)(PPh_3)_2]$ (1.291(6) and 1.296(6) Å),[11] $[Ru^{II}(trpy)(Bu_2SQ)Cl]$ (1.33(2) and 1.30(2) Å, 1.26(2) and 1.33(2) Å; two isomers),[16] and $[Ru^{II}(trpy)(3,6Bu_2SQ)(CO)]$ (3,6Bu_2SQ = 3,6-di-*tert*-butyl-1,2-benzosemiquinone; 1.283(9) and 1.301(8) Å).[25] The C1−O1 and C2−O2 bond lengths of **5** (1.35(1) and 1.34(1) Å) are longer than those of **1** but appear to be somewhat shorter than those of analogous aqua-metal complexes with Bu_2Cat such as $[Cr(trpy)(Bu_2Cat)(OH_2)](ClO_4)$ (1.361(3) and 1.377(3) Å) and $[Cr(metacn)(Bu_2Cat)(OH_2)](ClO_4)$ (metacn = 1,4,7-trimethyl-1,4,7-triazacyclononane; 1.366(3) and 1.364(3) Å).[26] Although the electronic structures of **1**, **3**, and **5** are not clearly defined by the C−O bond lengths, **1** and **5** showed a strong CT band at 870 nm, which was observed at 600 nm in the electronic spectrum of **3** (vide infra). Based on the fact that CT bands which emerged around 600 and 800 nm are associated with the oxidation states of eqs 2 and 3, respectively,[5−10] the actual stucture of **3** is close to the $[Ru^{III}(SQ)]$ structure of eq 2, and those of **1** and **5** lie close to the $[Ru^{II}(SQ)]$ ones in eq 3.

The Ru−OH_2 bond length (Ru−O3) of **3** (2.099(3) Å) is shorter than that of analogous aqua complexes of $[Ru^{II}(trpy)$-$(bpy)(OH_2)](ClO_4)_2$ (2.136(5) Å)[27] and $[Ru^{II}(dppe)(CO)(OSO_2$-$CF_3)_2(OH_2)]$ (dppe = 1,2-bis(diphenylphosphino)ethylene; 2.198(5) Å)[28] and $[Ru^{II}(Tp^{iPr})(THF)(X)(OH_2)]^{n+}$ (Tp^{iPr} = hydro-tris(3,5-diisopropylpyrazolyl)borate, X = THF, OH_2, py, *t*-BuCN, =C(=H)SiMe_3, etc.; 2.106(3)−2.189(6) Å).[29] The most striking character of the molecular structure of **5** is the Ru−O bond length 2.043(7) Å, which is shorter than the Ru−OH_2 bond distance of **3** but much longer than that of Ru−OH and the Ru=O bond length reported so far, such as $[Ru^{III}(metacn)(acac)$-$(OH)](PF_6)$ (1.971(9) Å)[30] for Ru−OH and $[Ru^{IV}(bpy)(DAMP)$-

deprotonated form of **3** was not soluble in H_2O, but it was soluble in a CH_3OH/H_2O mixture. We have successfully isolated the doubly deprotonated form of **3** as reddish purple crystals of neutral $[Ru^{II}(trpy)(Bu_2SQ)O^{\bullet-}]$ (**5**) (vide infra) by slow evaporation of CH_3OH from a CH_3OH/H_2O (1:2 v/v) solution of **3** under strong basic conditions. Treatment of **5** with 2.0 equiv of HClO_4 in CH_2Cl_2 regenerated **3** quantitatively. Moreover, the complex **5** has semiquinone and oxyl radical ligands, which show the antiferromagnetic interaction (vide infra).

Figure 1 shows the ORTEP views of **1**, **3**, and **5**.[24] The selected bond lengths of these complexes are listed in Table 2. The three complexes have a similar configuration; three nitrogen atoms of trpy and one oxygen of dioxolene are bonded to Ru in the equatorial plane, and the remaining one oxygen of dioxolene and another oxygen atom of an acetato (**1**), aqua (**3**), or oxo (**5**) ligands are linked to the central metal in the axial position.

(24) There are two possible isomers with respect to the orientation of 3,5-di-*tert*-butyldioxolene ligands of **1**, **3**, and **5**. Complexes depicted in Figure 1 predominantly crystallized under experimental conditions.
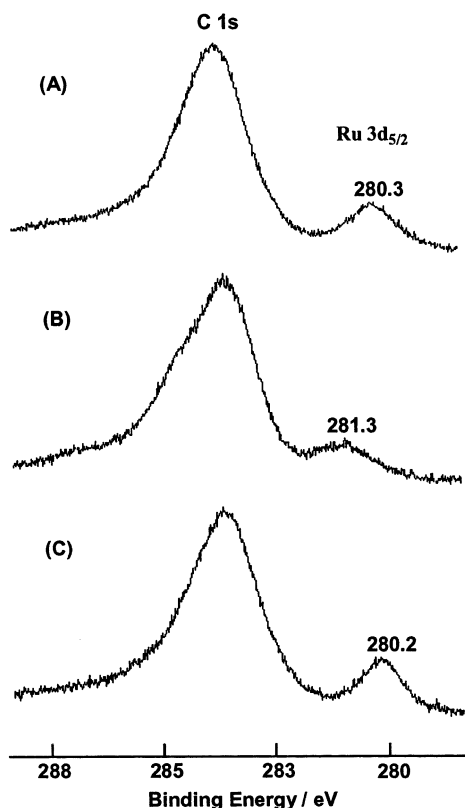
(25) Sugimoto, H.; Tanaka, K. *J. Organomet. Chem.* **2001**, *622*, 280.
(26) Shiren, K.; Tanaka, K. *Inorg. Chem.* **2002**, *41*, 5912.
(27) Seok, W. K.; Kim, M. Y.; Yokomori, Y.; Hodgson, D. J.; Meyer, T. J. *Bull. Korean Chem. Soc.* **1995**, *16*, 619.
(28) Mahon, M. F.; Whittlesey, M. K.; Wood, P. T. *Organometallics* **1999**, *18*, 4068.
(29) Takahashi, Y.; Akita, M.; Hikichi, S.; Moro-oka, Y. *Inorg. Chem.* **1998**, *37*, 3186.

Figure 2. XPS of **1** (A), **3** (B), and **5** (C) showing the binding energies of Ru $3d_{5/2}$ and C 1s. The C 1s reference peak is defined as 284.6 eV in all cases.

O]$(ClO_4)_2$ (DAMP = 2,6-bis((dimethylamino)methyl)pyridine; 1.805(3) Å),[31] [Ru^{IV}Cl(py)$_4$O]ClO$_4$ (1.862(8) Å),[32] and [Ru^{IV}X-(TMC)O]$^+$ (TMC = 1,4,8,11-tetramethyl-1,4,8,11-tetraazacyclotetradecane, X = Cl, N$_3$, and NCO; 1.765(5) Å)[33] for Ru=O. The Ru−oxyl bond of **5**, therefore, is classified as a single bond rather than a double bond. Thus, the neutral complex **5** is the first example of a terminal metal−O complex with a single bond character.[34]

X-ray Photoelectron Spectra. The C−O bond distances of coordinated dioxolene of **1**, **3**, and **5** did not always define the oxidation states of the ligands. So, we measured X-ray photoelectron spectra (XPS) in the range 274−296 eV to clarify the oxidation states of the Ru of these complexes. Peaks occurred in this region due to ruthenium (Ru $3d_{3/2}$ and Ru $3d_{5/2}$) and carbon (C 1s) electron transition. XPS data of the complex **1**, **3**, and **5** are shown in Figure 2. Binding energies for the Ru $3d_{5/2}$ peaks of the three complexes are listed in Table 3. For each complex, the Ru $3d_{3/2}$ peak could not be observed clearly, because the C 1s peak overlapped on the Ru$_{3/2}$ peak. The Ru $3d_{5/2}$ binding energies of **1** and **5** were 280.5 and 280.4 eV, respectively, which are in good agreement with the values for Ru^{II} $3d_{5/2}$ such as [Ru^{II}(bpy)$_2$Cl$_2$] (280.1 eV)[35] and [Ru^{II}(3Clpy)$_2$-(Bu$_2$SQ)$_2$] (280.4 eV).[36] Thus, **1** and **5** apparently have the Ru^{II} cores. The complex **3** showed the Ru$_{5/2}$ peak at 281.5 eV.

(30) Schneider, R.; Weyhermüller, T.; Wieghardt, K. *Inorg. Chem.* **1993**, *32*, 4925.
(31) Welch, T. W.; Ciftan, S. A.; White, P. S.; Thorp, H. H. *Inorg. Chem.* **1997**, *36*, 4812.
(32) Yukawa, Y.; Aoyagi, K.; Kurihara, M.; Shinai, K.; Shimizu, K.; Mukaida, M.; Takeushi, T.; Kakihara, H. *Chem. Lett.* **1985**, 283.
(33) Che, C.-M.; Lai, T.-F.; Wong, K.-Y. *Inorg. Chem.* **1987**, *26*, 2289.
(34) The O····O distance between two oxo groups of neighboring complexes was 6.64 Å, which is too long for any interaction.

Table 3. Ruthenium $3d_{5/2}$ Binging Energies

complex	Ru $3d_{5/2}$ (eV)	reference
[Ru^{II}(trpy)(Bu$_2$SQ)(OAc)]	280.5	*a*
[Ru^{II}(trpy)(4ClSQ)(OAc)]	280.4	*a*
[Ru^{III}(trpy)(Bu$_2$SQ)(OH$_2$)](ClO$_4$)$_2$	281.5	*a*
[Ru^{II}(trpy)(Bu$_2$SQ)O$^{\bullet -}$]	280.4	*a*
[Ru^{II}(bpy)$_2$Cl$_2$]	280.1	35
[Ru^{II}(3Clpy)$_2$(Bu$_2$SQ)$_2$]	280.4	36
[Ru^{III}(bpy)$_2$Cl$_2$]Cl	282.1	35
[Ru^{III}(3Clpy)$_2$(Bu$_2$SQ)$_2$]ClO$_4$	281.4	36
[Ru(NH$_3$)$_6$]Cl$_3$	282.1	37

a This work.
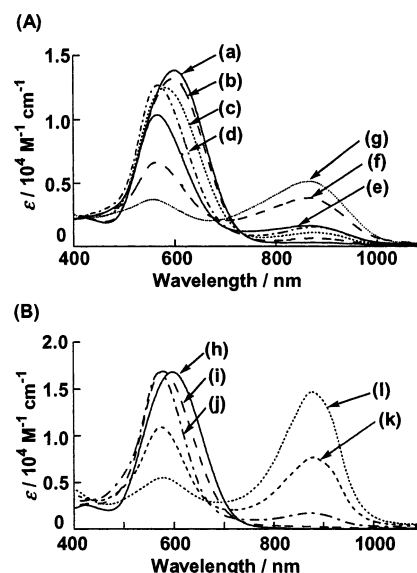
Figure 3. (A) pH dependent electronic absorption spectra of **3** (pH 3.2 (a); pH 4.5 (b); pH 5.6 (c); pH 7.1 (d); pH 10.1 (e); pH 11.0 (f); pH 12.0 (g)). (B) Electronic absorption spectra of **3** in the presence of various amounts of *t*-BuOK (0 equiv (h); 0.5 equiv (i); 1.0 equiv (j); 2.0 equiv (k); 3.0 equiv (l)) in CH$_2$Cl$_2$.

This value is significantly larger than those of Ru^{II} complexes and smaller than those of [Ru^{III}(bpy)$_2$Cl$_2$]Cl (282.1 eV)[35] and [Ru^{III}(NH$_3$)$_6$]Cl$_3$ (282.1 eV).[37] On the other hand, not only the C−O$_{av}$ bond distance of the dioxolene ligand (1.29 Å) but also the binding energy of **3** are quite close to those of [Ru^{III}(3Clpy)$_2$(Bu$_2$SQ)$_2$]ClO$_4$ (281.4 eV),[36] indicating that **3** has the [Ru^{III}(Bu$_2$SQ)] framework. The fact that the binding energy of the [Ru^{III}(Bu$_2$SQ)] core lies on the boundary between normal Ru^{II} and Ru^{III} complexes may reflect an occurrence of the resonance of eq 2.

Electronic Spectra. The electronic absorption spectra of complex **3** in water at pH 3.2 showed a strong absorption band at λ_{max} = 600 nm (ϵ = 13 800 M^{-1} cm^{-1}) (Figure 3A(a)). An increase of pH of the solution shifted the band maximum from 600 nm to 576 nm, and the absorbance at 576 nm reached the maximum at pH 7.1. Further alkalization of the solution resulted in an appearance of another band at 870 nm by decreasing the absorbance at the 576 nm band (Figure 3A). The intensity of 870 nm band observed at a pH higher than 10 is much weaker

(35) Weaver, T. R.; Meyer, T. J.; Adeyemi, S. A.; Brown, G. M.; Eckberg, R. P.; Hatfield, W. E.; Johnson, E. C.; Murray, R. W.; Untereker, D. *J. Am. Chem. Soc.* **1975**, *97*, 3039.
(36) Aubern, P. R.; Dodsworth, E. S.; Haga, M.; Liu, W.; Nevin, W. A.; Lever, A. P. B. *Inorg. Chem.* **1991**, *30*, 3502.
(37) Shepherd, R. E.; Proctor, A.; Henderson, W. W.; Myser, T. K. *Inorg. Chem.* **1987**, *26*, 2440.

than the 600 nm band of **3**, because of the insolubility of **5**, which is the doubly deprotonated form of **3**, in H_2O.

Although the solubility of **5** was too low to monitor the conversion from **3** to **5** in water, two successive equilibria of **3** were clearly observed in CH_2Cl_2 in the presence of various amounts of *t*-BuOK as a base (Figure 3B).[13] A strong absorption band at 600 nm ($\epsilon = 16\,800$ M^{-1} cm^{-1}) of **3** shifts to 576 nm upon a gradual addition of a 2-methoxyethanol solution of *t*-BuOK to the CH_2Cl_2 solution. The shift of the absorbance band around 600 nm reaches 576 nm ($\epsilon = 16\,700$ M^{-1} cm^{-1}) in the presence of 1.0 equiv of *t*-BuOK. Further addition of *t*-BuOK to the solution decreases the absorption of the 576 nm band, and a new band emerges at 870 nm. The 576 nm band almost disappeared in the presence of more than 3.0 equiv of *t*-BuOK. Moreover, acidification by an addition of 3.0 equiv of $HClO_4$ in 2-methoxyethanol to the solution fully recovered the electronic absorption spectrum of **3** ($\lambda_{max} = 600$ nm, $\epsilon = 16\,800$ M^{-1} cm^{-1}). Thus, the absorption maximum of **3** at 600 nm reversibly shifts to 576 nm and then to 870 nm in the presence of less than and more than 1.0 equiv of *t*-BuOK, respectively. Moreover, **5** obtained as single crystals also exhibited the same strong band at 870 nm in CH_2Cl_2, which completely disappeared by an addition of 2.0 equiv of $HClO_4$, and the 600 nm band of **3** was completely recovered.

The charge distribution between the $[Ru^{II}(Q)]$ and $[Ru^{III}(SQ)]$ frameworks (eq 2) and their one-electron reduced forms (eq 3) ($[Ru^{II}(SQ)]$ and $[Ru^{III}(Cat)]$) is associated with characteristic CT bands around 600 nm and 850 nm, respectively.[5−10] In fact, $[Ru^{III}(trpy)(Bu_2SQ)Cl]^+$ and $[Ru^{III}(trpy)(Bu_2SQ)(OAc)]^+$ exhibit the CT bands at 592 nm ($\epsilon = 15\,500$ M^{-1} cm^{-1}) and 584 nm ($\epsilon = 17\,000$ M^{-1} cm^{-1}),[16] while $[Ru^{II}(bpy)_2(Bu_2SQ)]^+$ and $[Ru^{II}(trpy)(Bu_2SQ)(OAc)]$ show those bands at 843 nm ($\epsilon = 15\,500$ M^{-1} cm^{-1})[7a] and 883 nm ($\epsilon = 18\,600$ M^{-1} cm^{-1}),[16] respectively. The shift of the CT band of **3** from 600 nm to 576 nm in the presence of less than 1.0 equiv of *t*-BuOK is simply explained by the formation of $[Ru^{III}(trpy)(Bu_2SQ)(OH^-)]^+$ (eq 4).

$$[Ru^{III}(trpy)(Bu_2SQ)(OH_2)]^{2+} \underset{+H^+}{\overset{-H^+}{\rightleftharpoons}}$$

$$[Ru^{III}(trpy)(Bu_2SQ)(OH)]^+ \underset{+H^+}{\overset{-H^+}{\rightleftharpoons}}$$
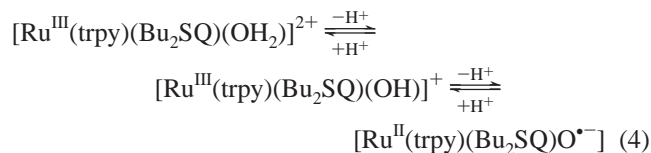
$$[Ru^{II}(trpy)(Bu_2SQ)O^{\bullet-}] \quad (4)$$

Accordingly, the appearance of the 870 nm band in the treatment of $[Ru^{III}(trpy)(Bu_2SQ)(OH_2)]^{2+}$ with more than 2.0 equiv of *t*-BuOK is indication of the occurrence of one-electron reduction of the $[Ru^{III}(Bu_2SQ)]$ core of **3** affording the $[Ru^{II}(Bu_2SQ)]$ one. The X-ray analysis and XPS of **5** demonstrated that the complex is expressed by $[Ru^{II}(trpy)(Bu_2SQ)O^{\bullet-}]$ (eq 4) rather than $[Ru^{III}(trpy)(Bu_2Cat)O^{\bullet-}]$.

One-electron reduction of the $[Ru^{III}(Bu_2SQ)]$ moiety of $[Ru^{III}(trpy)(Bu_2SQ)(OH^-)]^+$ coupled with dissociation of the hydroxo proton is caused by intramolecular electron transfer from the resultant negatively charged oxo group to the Ru−dioxolene moiety. Thus, Ru−dioxolene plays the key role as the electron reservoir in the acid−base equilibrium of the hydroxo ligand of $[Ru^{III}(trpy)(Bu_2SQ)(OH^-)]^+$ (eq 4).

The absorption spectrum of $[Ru^{III}(trpy)(4ClSQ)(OH_2)](ClO_4)_2$ (**4**) displays the strong CT band at 567 nm ($\epsilon = 5600$ M^{-1} cm^{-1}) in CH_2Cl_2 (Figure 4a). The absorbance at the 567 nm band is
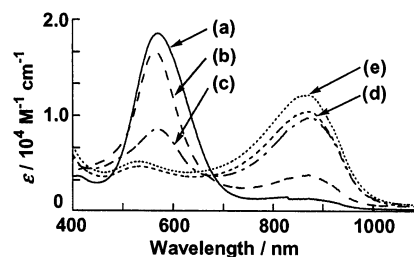
Figure 4. Electronic absorption spectra of **4** in the presence of various amounts of *t*-BuOK (0 equiv (a); 0.25 equiv (b); 0.5 equiv (c); 0.75 equiv (d); 1.0 equiv (e)) in CH_2Cl_2.
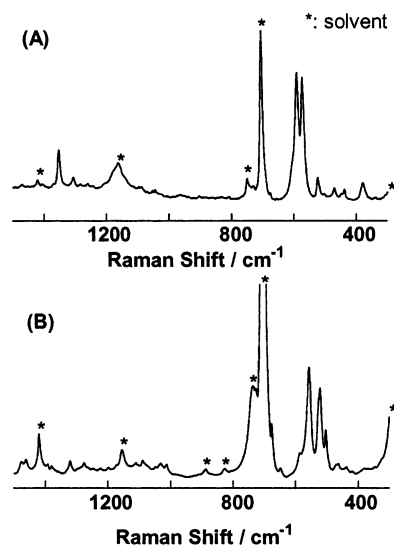
Figure 5. Resonance Raman spectra of **3** in CH_2Cl_2 at rt; 632.8 nm excitation (A) and 704.3 nm excitation (B) in the presence of 3.0 equiv of *t*-BuOK.

decreased by an addition of *t*-BuOK to the solution, and a new absorption band assignable to the CT band of the $[Ru^{III}(Cat)]$ or $[Ru^{II}(SQ)]$ moiety emerges at 870 nm ($\epsilon = 3700$ $M^{-1}cm^{-1}$), which become almost constant in the presence of ~1.0 equiv of *t*-BuOK. The treatment of **4** with 1.0 equiv of *t*-BuOK shifted the CT band from 567 to 870 nm, and no other strong absorption band was detected in the electronic spectra. One-electron reduction of 4-chlorosemiquinone of $[Ru^{III}(trpy)(4ClSQ)-(OH_2)]^+$, therefore, is induced by the first deprotonation of the aqua ligand in contrast to the equilibrium of eq 4.

Resonance Raman Spectra. Compounds **3** and **4** have the strong CT band at 600 and 567 nm, respectively, in CH_2Cl_2. The resonance Raman (rR) spectrum of **3** in the same solvent with a 632.8 nm excitation exhibits four strongly enhanced bands at 572, 590, 1167, and 1353 cm^{-1} and five weakly enhanced peaks at 382, 440, 472, 524, and 1309 cm^{-1} (Figure 5A).

The rR pattern of **3** resembles that of the one-electron oxidized form of $[Ru^{II}(bpy)_2(Bu_2SQ)]^+$ (516, 560, 585, 1072, 1125, and 1351 cm^{-1}).[38] According to the rR assignment of the oxidized form of $[Ru^{II}(bpy)_2(Bu_2SQ)]^+$, the two strong bands at 572 and 590 cm^{-1} of **3** are correlated with Ru−O stretching modes coupled with the $\nu(C-C)$ and ring deformation modes, indicating strong electronic influence of the CT band of Ru−dioxolene on the Ru−O bonds ($[Ru^{II}(Bu_2Q)]$ or $[Ru^{II}(Bu_2SQ)]$). The remaining two enhanced peaks (1167 and 1353 cm^{-1}) are
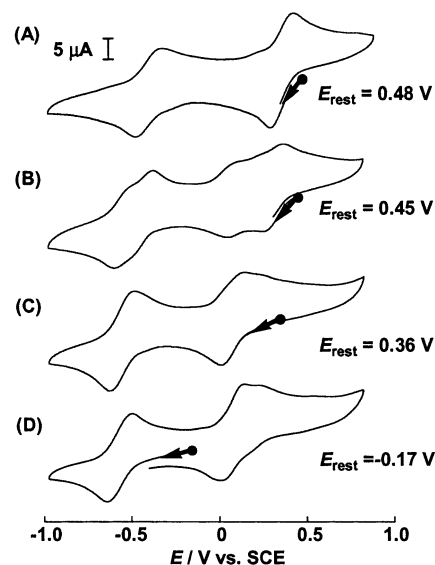
(38) Stufkens, D. J.; Snoeck, Th. L.; Lever, A. P. B. *Inorg. Chem.* **1988**, *27*, 953.

assigned to the stretching modes of the dioxolene ligand.[38] The Raman spectrum of **4** is also close to that of the oxidized form of $[Ru^{II}(bpy)_2(Bu_2SQ)]^+$, but all observed peaks at 380, 440, 478, 521, 549, 590, 1160, and 1367 cm^{-1} are not so enhanced compared with those of the rR spectrum of **3**. This is because the wavelength of the excitation laser 632.8 nm is far from the CT band of **4** at 567 nm. The bands at 549 and 590 nm and those at 1160 and 1367 cm^{-1} are also associated with the stretching modes of Ru−O bonds and the dioxolene ligands, respectively. Thus, the rR spectra of **3** and **4** are identification of the resonance form of eq 2.

As described in a previous section, **5** displays the strong CT band at 870 nm in CH$_2$Cl$_2$. No Raman peak of **5**, that was prepared by the reaction of **3** with 3.0 equiv of t-BuOK in CH$_2$-Cl$_2$, was detected with a 632.8 nm excitation, but the rR spectrum of **5** in the same solvent exhibited 10 weakly enhanced peaks at 503, 521, 556, 590, 1157, 1280, 1324, 1467, 1481, and 1497 cm^{-1} with a 704.3 nm excitation (Figure 5B). The five bands at 1157, 1280, 1467, 1481, and 1497 cm^{-1} are tentatively associated with the stretching vibrations of the Ru−trpy framework from the similarity of the rR spectra of $[Ru^{II}-(trpy)_2](PF_6)_2$ which showed strong peaks at 1164, 1284, 1470, 1490, and 1549 cm^{-1} in CH$_2$Cl$_2$.[39] The four peaks at 503, 521, 556, and 590 cm^{-1} of **5** are correlated with the ν(Ru−O) bands coupled with the ν(C−C) bands of the dioxolene ligand by reference to the bands of $[Ru^{II}(bpy)_2(Bu_2SQ)]^+$ (519 and 551 cm^{-1})[38] and $[Ru^{II}(trpy)(Bu_2SQ)(OAc)]$ (**1**) (504, 521, 558, and 593 cm^{-1}). The remaining 1324 cm^{-1} peak of **5** is assigned to the ν(C−O) mode of the dioxolene ligand, because the ν(C−O) bands of $[Ru^{II}(bpy)_2(Bu_2SQ)]$ and $[Ru^{II}(trpy)(Bu_2SQ)(OAc)]$ were observed at 1315 cm^{-1} and 1324 cm^{-1}, respectively. Similarly, the rR spectrum of **4** in CH$_2$Cl$_2$ in the presence of 3.0 equiv of t-BuOK exhibited quite weakly enhanced peaks at 467, 504, 533, and 1325 cm^{-1} due to the $[Ru^{II}(SQ)]$ or $[Ru^{III}-(Cat)]$ framework with a 704.3 nm excitation, and the pattern was close to those of not only **5** but also $[Ru^{II}(bpy)_2(Bu_2SQ)]^+$ and $[Ru^{II}(trpy)(Bu_2SQ)(OAc)]$ in the same solvent.

Electrochemistry. The cyclic voltammograms (CVs) of **3** in the presence of various amounts of t-BuOK are shown in Figure 6. The $E_{1/2}$ value and the rest potential (or equilibrium electrode potential) of the solution (E_{rest}) are summarized in Table 4.

The CV of **3** in CH$_2$Cl$_2$ exhibits two reversible redox waves at $E_{1/2}^{1a} = 0.31$ V and $E_{1/2}^{1b} = -0.47$ V (vs SCE). Taking into account that **3**, the hydroxy complex, and **5** have the $[Ru^{II}(Bu_2SQ)]$, $[Ru^{III}(Bu_2SQ)]$, and $[Ru^{II}(Bu_2SQ)]$ cores, respectively (eq 4), we assume the one-electron reduction of **3** and the hydroxo complex to give the $[Ru^{II}(Bu_2SQ)]$ core rather than the $[Ru^{III}(Bu_2Cat)]$ one. The redox reactions of **3** at 0.31 V and −0.47 V, therefore, are associated with the $[Ru^{III}(Bu_2SQ)]^{2+}/[Ru^{II}(Bu_2SQ)]^+$ and $[Ru^{II}(Bu_2SQ)]^+/[Ru^{II}(Bu_2Cat)]$ couples. The addition of 1.0 equiv of t-BuOK into the solution resulted in the disappearance of the $E_{1/2}^{1a} = 0.31$ V and $E_{1/2}^{1b} = -0.47$ V redox couples (Figure 6C). Instead, new two redox couples emerged at $E_{1/2}^{2a} = 0.07$ V and $E_{1/2}^{2b} = -0.57$ V, which are assigned to the $[Ru^{III}(Bu_2SQ)]^{2+}/[Ru^{II}(Bu_2SQ)]^+$ and $[Ru^{II}(Bu_2SQ)]^+/[Ru^{II}(Bu_2Cat)]$ couples of $[Ru^{III}(trpy)(Bu_2SQ)(OH^-)]^+$. The rest potentials ($E_{rest}$) of **3** and $[Ru^{III}(trpy)(Bu_2SQ)(OH^-)]^+$

(39) Coe, B. J.; Tompson, D. W.; Culbertson, C. T.; Schoonover, J. R.; Meyer, T. J. *Inorg. Chem.* **1995**, *34*, 3385.

Figure 6. Cyclic voltammograms of **3** (1.0 mM) in the presence of various amounts of t-BuOK in CH$_2$Cl$_2$: 0 equiv, $E_{rest} = 0.48$ V (A); 0.5 equiv, $E_{rest} = 0.45$ V (B); 1.0 equiv, $E_{rest} = 0.36$ V (C); 3.0 equiv, $E_{rest} = -0.17$ V (D).

Table 4. Redox Potentials (V vs SCE) and Rest Potentials (V) for Complexes **3** and **4** under Various Conditions

	$[Ru^{III}(R_nSQ)]^{2+}/$ $[Ru^{II}(R_nSQ)]^+$	$[Ru^{II}(R_nSQ)]^+/$ $[Ru^{II}(R_nCat)]$	E_{rest}
3	0.31	−0.47	0.48
3 + 1.0 equiv of t-BuOK	0.07	−0.57	0.36
3 + 3.0 equiv of t-BuOK	0.07	−0.57	−0.17
4	0.60	−0.14	0.71
4 + 1.0 equiv of t-BuOK	0.29	−0.48	−0.17

in CH$_2$Cl$_2$ are 0.48 and 0.36 V, respectively, which also manifest the $[Ru^{III}(Bu_2SQ)]^{2+}$ structure of both complexes, because the E_{rest} is located at potentials more positive than those of the $[Ru^{III}(Bu_2SQ)]^{2+}/[Ru^{II}(Bu_2SQ)]^+$ redox couple of both complexes ($E_{1/2}^{1a} = 0.31$ V, $E_{1/2}^{2a} = 0.07$ V). The redox couples at $E_{1/2}^{2a} = 0.07$ V and $E_{1/2}^{2b} = -0.57$ V of $[Ru^{III}(trpy)(Bu_2SQ)-(OH^-)]^+$ in CH$_2$Cl$_2$ were hardly influenced by the addition of more than 1.0 equiv of t-BuOK to the solution, but E_{rest} of the solution dramatically shifted from +0.48 to −0.17 V passing through the $[Ru^{III}(Bu_2SQ)]^{2+}/[Ru^{II}(Bu_2SQ)]^+$ redox couple of $[Ru^{III}(trpy)(Bu_2SQ)(OH^-)]^+$ at $E_{1/2}^{2a} = 0.07$ V (Figure 6D). Such characteristic behavior is explained by the view that the first deprotonation of $[Ru^{III}(trpy)(Bu_2SQ)(OH_2)]^{2+}$ just converts the aqua ligand (OH$_2$) to the hydroxo one (OH$^-$), and the subsequent deprotonation of the hydroxo ligand (OH$^-$) of $[Ru^{III}(trpy)(Bu_2SQ)(OH^-)]^+$ causes electron transfer from the resultant O^{2-} to $[Ru^{III}(Bu_2SQ)]^{2+}$ yielding an oxyl radical (O$^{\bullet-}$) and $[Ru^{II}(Bu_2SQ)]^+$ of **5** (Scheme 1A). Indeed, **5** generated by deprotonation of $[Ru^{III}(trpy)(Bu_2SQ)(OH^-)]^+$ exhibits the characteristic CT band of the $[Ru^{II}(Bu_2SQ)]^+$ framework at 870 nm. The Ru−OH$_2$ complex **3**, Ru−OH complex $[Ru^{III}(trpy)-(Bu_2SQ)(OH^-)]^+$, and Ru−O$^{\bullet-}$ one show their own electronic absorption spectra. On the other hand, the redox potentials of the $[Ru^{III}(Bu_2SQ)]^{2+}/[Ru^{II}(Bu_2SQ)]^+$ and the $[Ru^{II}(Bu_2SQ)]^+/[Ru^{II}(Bu_2Cat)]$ couples of $[Ru^{III}(trpy)(Bu_2SQ)(OH^-)]^+$ closely resembles those of **5**, suggesting that OH$^-$ and O$^{\bullet-}$ give similar electronic influence on the redox reaction of the Ru−dioxolene moiety. Moreover, the redox potentials of **5** were hardly influenced by the presence of free t-BuOK, because **5** isolated

Scheme 1

(A) [Ru^{III}(trpy)(Bu$_2$SQ)(OH$_2$)]$^{2+}$


(B) [Ru^{III}(trpy)(4ClSQ)(OH$_2$)]$^{2+}$
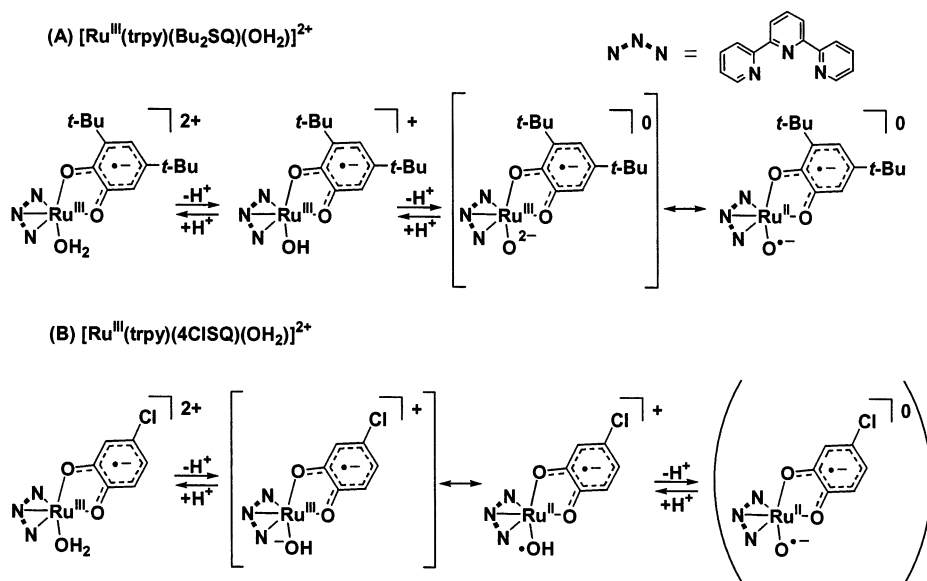
as reddish purple crystals displayed the same CV as that of **3** in the presence of 3.0 equiv of *t*-BuOK in CH$_2$Cl$_2$.

The CV of **4** in CH$_2$Cl$_2$ also showed the two reversible redox waves at $E_{1/2}^{1a} = 0.60$ V and $E_{1/2}^{1b} = -0.14$ V (vs SCE). The electronic structures of the acetato complex **2**, aqua complex **4**, and the oxo complex derived from double deprotonation of **4** are described as [Ru^{II}(trpy)(4ClSQ)(OAc)],[17] [Ru^{III}(trpy)(4ClSQ)-(OH$_2$)]$^{2+}$, and [Ru^{II}(trpy)(4ClSQ)(O$^{•-}$)] (vide infra), respectively, suggesting that one-electron reduction of **4** takes place on the central metal. The redox reactions at $E_{1/2}^{1a} = 0.60$ V and $E_{1/2}^{1b} = -0.14$ V, therefore, are ascribed to the [Ru^{III}-(4ClSQ)]$^{2+}$/[Ru^{II}(4ClSQ)]$^{+}$ and [Ru^{II}(4ClSQ)]$^{+}$/[Ru^{II}(4ClCat)] couples, respectively. The peak currents of these redox waves decreased upon an addition of *t*-BuOK to the solution. Instead, one quasi-reversible and one reversible redox couple of the corresponding hydroxy complex appeared at $E_{1/2}^{2a} = 0.29$ V and $E_{1/2}^{2b} = -0.48$ V (vs SCE), respectively. At the same time, the rest potential negatively shifted from 0.71 V to -0.17 V passing through the quasi-reversible couple of the hydroxy complex at $E_{1/2}^{2a} = 0.29$ V. The change of CV almost ceased after the addition of 1.0 equiv of *t*-BuOK. Deprotonation of the aqua ligand of **4**, therefore, probably produces [Ru^{II}(trpy)-(4ClSQ)(OH$^{•}$)]$^{+}$ rather than [Ru^{III}(trpy)(4ClSQ)(OH^{-})]$^{+}$ (Scheme 1B).

In contrast to the equilibrium of eq 4, the deprotonation of the aqua ligand of **4** induces intramolecular electron transfer from OH^{-} to the [Ru^{III}(4ClSQ)] framework giving [Ru^{II}(trpy)-(4ClSQ)(OH$^{•}$)]$^{+}$. The absence of an isosbestic point in the conversion from **4** to [Ru^{II}(trpy)(4ClSQ)(OH$^{•}$)]$^{+}$ (Figure 4) may be associated with a concomitant intermolecular electron transfer from the resultant [Ru^{II}(trpy)(4ClSQ)(OH$^{•}$)]$^{+}$ to unreacted [Ru^{III}-(trpy)(4ClSQ)(OH$_2$)]$^{2+}$ (eq 5).

$$[\text{Ru}^{II}(\text{trpy})(4\text{ClSQ})(\text{OH}^{•})]^{+} + [\text{Ru}^{III}(\text{trpy})(4\text{ClSQ})(\text{OH}_2)]^{2+} \rightarrow$$

$$[\text{Ru}^{III}(\text{trpy})(4\text{ClSQ})(\text{OH}^{•})]^{2+} + [\text{Ru}^{II}(\text{trpy})(4\text{ClSQ})(\text{OH}_2)]^{+} \quad (5)$$
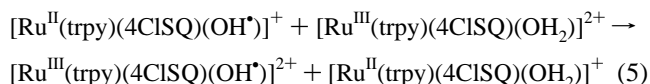
Spin Trapping Experiments. The complex **3** did not show any EPR signals in CH$_2$Cl$_2$. An addition of more than 1.0 equiv of *t*-BuOK to the solution resulted in an appearance of an isotropic broad signal ($g = 2.030$, $\Delta H_{msl} = 8.0$ mT) without a hyperfine

structure at 193 K. The intensity of the signal linearly increased with an increase of the amount of *t*-BuOK and became almost constant in the presence of 3.0 equiv of the base. The isotropic broad signal centered at $g = 2.029$ would be correlated with the triplet state, and the absence of hyperfine structures probably resulted from the solution state measurements (vide infra). The technique of spin trapping using 5,5-dimethl-1-pyrroline *N*-oxide (DMPO) was applied for detection and identification of the oxyl radical moiety of [Ru^{II}(trpy)(Bu$_2$SQ)O$^{•-}$], which is produced in the reaction of **3** with 3.0 equiv of *t*-BuOK in CH$_2$Cl$_2$. Indeed, 12-line sharp signals centered at $g = 2.006$ together with the isotropic broad signal without a hyperfine structure ($g = 2.029$, $\Delta H_{msl} = 7.3$ mT) are detected in the EPR spectrum of a CH$_2$-Cl$_2$ solution containing **3** and 3.0 equiv of *t*-BuOK and of DMPO (Figure 7A).

The appearance of the 12-line sharp signals demonstrates the spin adduct formation between [Ru^{II}(trpy)(Bu$_2$SQ)O$^{•-}$] (**5**) and DMPO, since the isotropic EPR signal of [Ru^{II}(trpy)(Bu$_2$SQ)-(OAc)] in CH$_2$Cl$_2$ ($g = 2.030$, $\Delta H_{msl} = 8.0$ mT) was not influenced by the presence of a large excess of DMPO. Moreover, purified **5** in the presence of excess amounts of DMPO also showed the same 12-line sharp signals in CH$_2$Cl$_2$.[40] The hyperfine coupling constants for the 12-line signals were determined as $a_N^{\alpha} = 1.35$, $a_H^{\beta} = 0.66$, and $a_H^{\gamma} = 0.15$ mT by the computer simulation, and the assignment of the EPR signal of the spin adduct, [Ru^{II}(trpy)(Bu$_2$SQ)(O-DMPO)], is depicted in Figure 8.

Similar 12-line signals of the spin adduct were also observed in the EPR spectra of a mixture of **4** and 3.0 equiv of *t*-BuOK and of DMPO in CH$_2$Cl$_2$ at 193 K (Figure 7B and C). The hyperfine coupling constants were also estimated as $a_N^{\alpha} = 1.30$, $a_H^{\beta} = 0.63$, and $a_H^{\gamma} = 0.21$ mT by the computer simulation (Figure 7D). On the other hand, a signal expected from the triplet state was not detected irrespective of the presence and the absence of DMPO.

The a_N^{α}, a_H^{β}, and a_H^{γ} values of the spin adducts are also summarized in Table 5. The a_N^{α} values of the spin adducts of Ru

---

(40) The signal of the DMPO spin adduct increased linearly with an increase in the DMPO concentration.
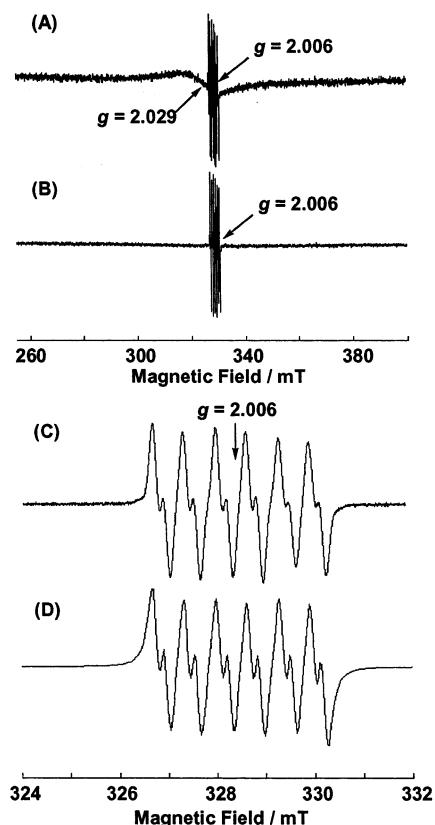
Figure 7. EPR spectra obtained upon the addition of 3.0 equiv of *t*-BuOK and of DMPO to a CH₂Cl₂ solution of **3** (2.0 mM (A)) and **4** (2.0 mM (B and C)) at 193 K. Shown in part D is a computer simulation of [Ru^{II}(trpy)-(4ClSQ)(O-DMPO)] ($g = 2.006$, $a_N^\alpha = 1.30$, $a_H^\beta = 0.63$, and $a_H^\gamma = 0.21$ mT). Microwave power is 1.0 mW, and modulation amplitude is 0.14 mT.
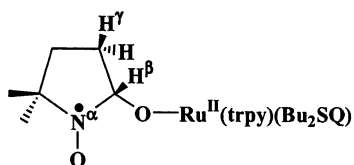
Figure 8. Proposed structure of DMPO spin adduct with the oxyl radical complex.

Table 5. Hyperfine Coupling Constants (mT) of DMPO Spin Adducts

parent radical	a_N^α	a_H^β	a_H^γ	reference
[Ru^{II}(trpy)(Bu₂SQ)(O$^{\bullet-}$)]	1.35	0.66	0.15	*a*
[Ru^{II}(trpy)(4ClSQ)(O$^{\bullet-}$)]	1.30	0.63	0.21	*a*
·OH	1.53	0.06		41
·OOH	1.43	1.17	0.13	41
·CH₂OH	1.60	2.27		42
CH₃·CHOH	1.58	2.28		42
·CH₂CO₂H	1.61	2.28		43
·CH₂CO₂⁻	1.61	2.28		43

ᵃ This work.

oxyl radical complexes are close to those of other spin adducts such as DMPO–OH (1.4–1.5 mT), though the a_H^β and a_H^γ values are largely influenced by parent radicals (Table 5).[41–43]

The 1:1 adduct formation between **5** and DMPO is further demonstrated by electron spray ionization mass spectroscopy

(41) Harbour, J. R.; Chow, V.; Bolton, J. R. *Can. J. Chem.* **1974**, *52*, 3549.
(42) Finkelstein, E.; Rosen, G. M.; Rauckman, E. J. *Arch. Biochem. Biophys.* **1980**, *200*, 1.
(43) Taniguchi, H.; Madden, K. P. *J. Phys. Chem.* **1998**, *102*, 6753.
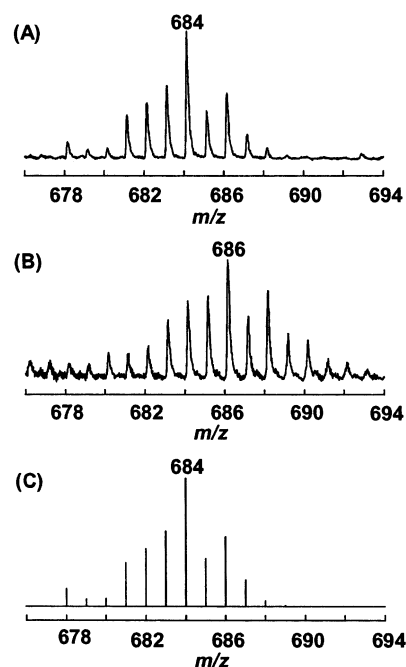
Figure 9. ESI mass spectra observed upon the addition of 3.0 equiv of *t*-BuOK and 100 equiv of DMPO into CH₂Cl₂ solution of **3** (10 mM) containing a small amount of water (H₂¹⁶O (A) and H₂¹⁸O (B)). Computer simulation of [Ru^{II}(trpy)(Bu₂SQ)(¹⁶O-DMPO)] (C).

(ESIMS). The mass spectrum of a CH₂Cl₂ solution containing **3**, 3.0 equiv of *t*-BuOK, and 100 equiv of DMPO (Figure 9A) well coincides with the simulated isotope pattern of [Ru^{II}(trpy)-(Bu₂SQ)(¹⁶O-DMPO)]⁺ (Figure 9C). The labeling experiment using [Ru^{III}(trpy)(Bu₂SQ)(¹⁸OH₂)](ClO₄)₂ under otherwise the same conditions also exhibited the expected signal at *m/z* 686 of [Ru^{II}(trpy)(Bu₂SQ)(¹⁸O-DMPO)]⁺ (Figure 9B). These observations also indicate the spin adduct formation between the oxyl radical of [Ru^{II}(trpy)(Bu₂SQ)O$^{\bullet-}$] and DMPO.

EPR Spectra at 3.9 K ($g = 2$). Both **3** and **4** in CH₂Cl₂ did not show any EPR signals at 3.9 K, suggesting antiferromagnetic interaction between Ru(III) and semiquinone. The EPR spectrum of a mixture of **3** and 3.0 equiv of *t*-BuOK at 3.9 K exhibited an isotropic broad signal with a hyperfine structure at the $\Delta m_s = 1$ region and an isotropic signal at $\Delta m_s = 2$, indicating the triplet state of a biradical compound (Figure 10A).[44–47] The hyperfine structure of zero field splitting at the $\Delta m_s = 1$ region is not observed clearly because of the large signal line width. The computer simulation curve of the triplet signal at the $\Delta m_s = 1$ region using WINEPR SimFonia verion 1.25 with $g_{xx} = g_{yy} = g_{zz} = 2.054$, $|D| = 0.020$ cm^{-1}, and $|E| = 0.005$ cm^{-1} gives good agreement with the observed spectrum. If D is assumed to involve only dipolar interaction, $|D|$ (cm^{-1}) is expressed as

$$D = -3g^2\beta^2/2r^3 \qquad (6)$$

by eq 6, where r (Å) is the spin–spin distance.[46] Calculation of eq 6 using $|D| = 0.020$ cm^{-1} and $g = 2.054$ afforded the

(44) A CH₂Cl₂/2-methoxyethanol (10:1 v/v) solution of **5** also showed the EPR signal of Figure 10A at 3.9 K.
(45) (a) Sheltz, D. A.; Bodnar, S. H. *Inorg. Chem.* **1999**, *38*, 591. (b) Shultz, D. A.; Lee, H.; Gawltney, K. P. *J. Org. Chem.* **1998**, *63*, 7584.
(46) Eaton, S. S.; More, K. M.; Sawant, B. M.; Eaton, G. R. *J. Am. Chem. Soc.* **1983**, *105*, 6560.
(47) (a) Gambarelli, S.; Jaouen, D.; Rassat, A. *J. Phys. Chem.* **1996**, *100*, 9605. (b) Pezeshk, A.; Coffman, R. E. *J. Phys. Chem.* **1986**, *90*, 6638.

(A)

Exp.

Sim.

Magnetic Field / mT

(B)

Exp.

Sim.

Magnetic Field / mT
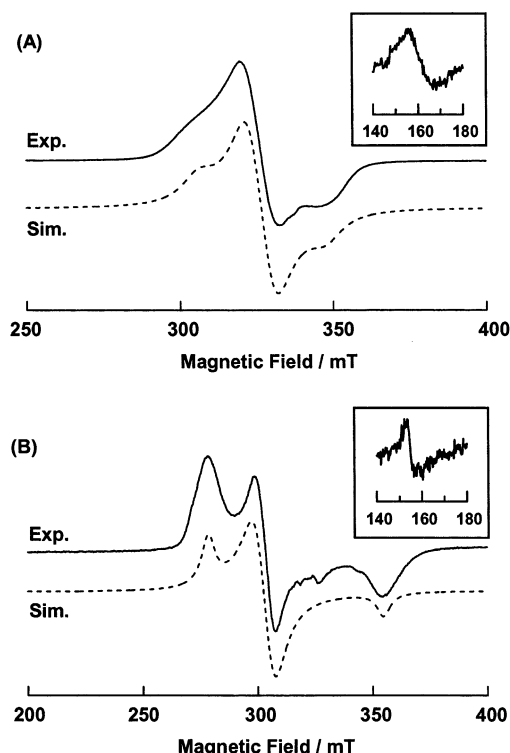
Figure 10. (A) EPR spectrum of **3** in the presence of 3.0 equiv of *t*-BuOK in CH$_2$Cl$_2$ at 3.9 K (solid line) and the simulation curve using $|D|$ = 0.020 cm^{-1}, $|E|$ = 0.005 cm^{-1}, and $g_{xx} = g_{yy} = g_{zz}$ = 2.054 (dashed line). (B) EPR spectrum of **4** in the presence of 3.0 equiv of *t*-BuOK in CH$_2$Cl$_2$ at 3.9 K (solid line) and simulation curve using $|D|$ = 0.038 cm^{-1}, $|E|$ = 0.011 cm^{-1}, $g_{xx} = g_{yy}$ = 2.150, and g_{zz} = 2.060 (dashed line).
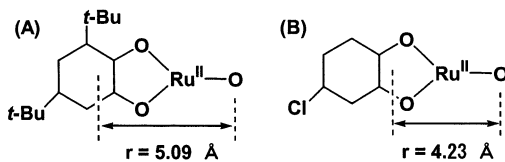

Figure 11. Calculated spin—spin distances of [Ru^{II}(trpy)(Bu$_2$SQ)(O$^{\bullet-}$)] (A) and [Ru^{II}(trpy)(4ClSQ)(O$^{\bullet-}$)] (B).

value 5.09 Å as the spin—spin distance. This value also strongly supports that **5** has an oxyl radical and a semiquinone one located in the aromatic ring of the dioxolene ligand based on the crystal structure of the complex (Figure 11).

The EPR spectrum of **4** at 3.9 K in the presence of 3.0 equiv of *t*-BuOK in frozen CH$_2$Cl$_2$ showed an anisotropic broad signal with a hyperfine structure of zero field splitting at the Δm_s = 1 region and an isotropic signal at Δm_s = 2. Computer simulation gives the EPR parameters $g_{xx} = g_{yy}$ = 2.150, g_{zz} = 2.060, $|D|$ = 0.038 cm^{-1}, and $|E|$ = 0.011 cm^{-1}. The spin—spin distance calculated from eq 1 using g_{av} = 2.12 and $|D|$ = 0.038 cm^{-1} is 4.23 Å, which indicates that two unpaired electrons are located at the oxygen atom of the oxo group and in the O—C—C—O chelate ring of the dioxolene ligand. Thus, the oxo complex derived from **4** has the [Ru^{II}(4ClSQ)O$^{\bullet-}$] framework rather than the [Ru^{III}(4ClCat)O$^{\bullet-}$] one (Figure 11). However, an anisotropic g value and a short spin—spin distance of [Ru^{II}(trpy)(4ClSQ)O$^{\bullet-}$] compared with those of **5** imply that the resonance of the oxo complex derived from **4** lies to the right ([Ru^{III}(Cat)]) of eq 7. Such a difference apparently results
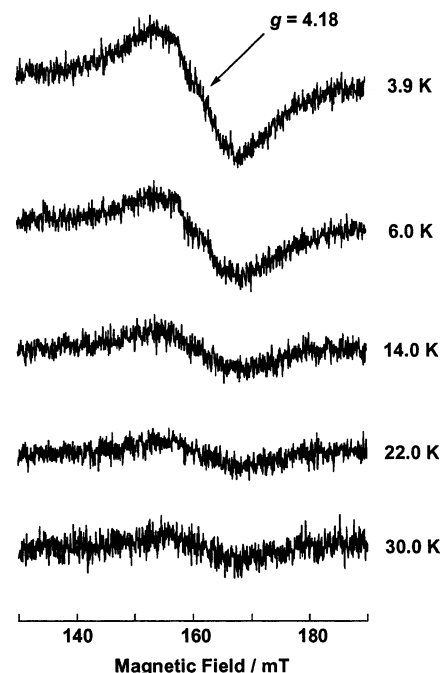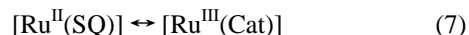
Figure 12. Temperature dependent EPR spectra of a CH$_2$Cl$_2$ solution of **3** containing 3.0 equiv of *t*-BuOK.
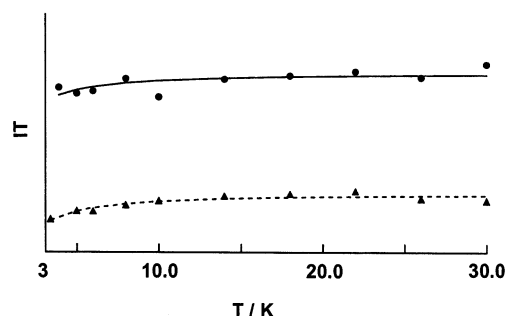
Figure 13. IT—*T* plot of the EPR spectra of **3** (●) and **4** (▲) in CH$_2$Cl$_2$ containing 3.0 equiv of *t*-BuOK. Simulation curves for **3** (solid line) and for **4** (dashed line).

from the strong electron withdrawing ability of 4ClSQ compared with Bu$_2$SQ.

$$[Ru^{II}(SQ)] \leftrightarrow [Ru^{III}(Cat)] \qquad (7)$$

Temperature Dependent EPR Spectra (g = 4). The EPR spectra of **3** and **4** in the presence of 3.0 equiv of *t*-BuOK in frozen CH$_2$Cl$_2$ exhibited signals at g = 4.18 and g = 4.65, respectively, due to the intramolecular magnetic interaction between [Ru^{II}(SQ)] and oxyl radicals. The intensities of the signals of **3** and **4** with base decrease with an increase of temperature (Figure 12).

The splitting energy 2*J* between the triplet and singlet is determined from the temperature dependence of intensities (IT vs *T*) by a fitting procedure to the Bleaney—Bowers equation IT = const.$(3 + \exp(-2J/kT))^{-1}$ ($H = -2JS_1S_2$) (Figure 13).[48] 2*J* values of **5** (**3** in the presence of 3.0 equiv of *t*-BuOK) and [Ru^{II}(trpy)(4ClSQ)O$^{\bullet-}$] are −0.67 cm^{-1} and −1.97 cm^{-1}, respectively.[48] The difference in the antiferromagnetic interaction

---

(48) *J* values obtained from the EPR signal intensities around g = 2 of **5** and [Ru^{II}(trpy)(4ClSQ)O$^{\bullet-}$] were essentially consistent with those of the values determined from signals around g = 4.

between the $[Ru^{II}(trpy)(4ClSQ)O^{\bullet-}]$ framework ($2J = -1.97$ cm^{-1}) and the $[Ru^{II}(trpy)(Bu_2SQ)O^{\bullet-}]$ one ($2J = -0.67$ cm^{-1}) is correlated to the short the spin−spin distance of $[Ru^{II}(trpy)(4ClSQ)O^{\bullet-}]$ compared with that of $[Ru^{II}(trpy)(Bu_2SQ)O^{\bullet-}]$.

Conclusion

Ru−OH$_2$ complexes containing a semiquinone ligand (**3**, **4**) reversibly dissociate protons to afford Ru−OH (or Ru−OH$^{\bullet}$) and Ru−O$^{\bullet-}$ (**5**) complexes. The Ru−O$^{\bullet-}$ complex **5** was isolated as single crystals by slow evaporation of CH$_3$OH of a CH$_3$OH/H$_2$O solution of **3** under strong basic conditions. The X-ray crystal structure revealed that **5** is the first terminal metal−O complex with a single bond length. Dissociation of a hydroxyl (or aqua) proton of **3** (or **4**) gave rise to the intra-molecular electron transfer from O^{2-} (or OH$^-$) to the $[Ru^{III}(SQ)]$ moiety, which resulted in the formation of an oxyl radical O$^{\bullet-}$ (or hydroxyl radical OH$^{\bullet}$) and the $[Ru^{II}(SQ)]$ core. The resulted Ru−oxyl radical complexes showed antiferromagnetic behavior, and the ruthenium−oxyl radical frameworks were characterized by spin trapping techniques. Ru−dioxolene plays the key roles in not only dissociation of hydroxyl proton as the electron reservoir but also stabilization of the triplet state of the $[Ru^{II}(SQ)]$ framework and oxyl radical ligand. This work is the first example of the metal complexes with an oxyl radical ligand and may shed light on the development of a new type of electrocatalysts.

Supporting Information Available: An X-ray crystallo-graphic file (CIF) of complex **1**, **3**, and **5**. This material is available free of charge via the Internet at http://pubs.acs.org.

JA0211510